

## DYNAMIC COMPRESSIBILITY AND EQUATION OF STATE OF IRON UNDER HIGH PRESSURE

L. V. AL' TSHULER, K. K. KRUPNIKOV, B. N. LEDENEV, V. I. ZHUCHIKHIN and M. I. BRAZHNIK

Submitted to JETP editor December 28, 1957

J. Exptl. Theoret. Phys. (U.S.S.R.) **34**, 874-885 (April, 1958)

Two methods for measurement of the dynamic compressibility of solids are described which are based on determination of the kinematic parameters of shock waves, — their velocity of propagation and the mass velocity of the substance behind the front. The adiabates of shock compression of iron possessing various initial densities were determined by these methods in the pressure range from  $4 \times 10^5$  to  $5 \times 10^6$  atm. The compressibility curve of iron at absolute zero is derived from the experimental data. The curve is extrapolated to pressures at which statistical atomic models are valid.

## INTRODUCTION

THE investigations of the equations of state of elements and compounds at high pressures are of great interest for various branches of experimental and theoretical physics, geophysics, cosmogony and a number of related disciplines.

Until recently, the only experimental method for the high-pressure region was the static measurement of compressibility using piezometers of various designs. Bridgman's well-known work<sup>1-3</sup> covered the range of pressures up to 100,000 atm. At still higher pressures the piezometer vessels were deformed so that exact measurements could not be obtained.

In an entirely different manner, which does not involve the use of mechanical pressure or special piezometers, conditions of high hydrostatic pressure are created for short time intervals behind the front of a strong shock wave. This method can be used to produce pressures of hundreds of thousands and millions of atmospheres, which are unattainable by static methods. The laws of mass and momentum conservation relate pressure and density in a shock compression to the kinematic parameters of the shock wave through two equations:

$$\sigma_1 = v_0 / v_1 = D / (D - U_1), \quad (1a)$$

$$P_1 = U_1 D / v_0, \quad (1b)$$

where  $D$  is the velocity of propagation of the shock wave,  $U_1$  is the mass (or particle) velocity of the material,  $v_1$  is the specific volume behind the shock front,  $v_0$  is the initial specific volume,  $\sigma_1$  is the relative compression and  $P_1$  is the pressure of the shock compression. It is assumed that ahead of the front the pressure is zero and the medium is at rest.

By means of Eqs. (1a) and (1b), the problem of determining pressures and densities  $p_1 = 1/v_1$  reduces to experimentally feasible measurements of the wave and mass velocities of shock waves.

We now consider the conservation of energy. The total amount of work done on a unit of mass by a passing shock front is represented in Fig. 1 by the area of the rectangle with the sides  $P_1$  and  $v_0 - v_1$ . According to Eqs. (1a) and (1b), half of

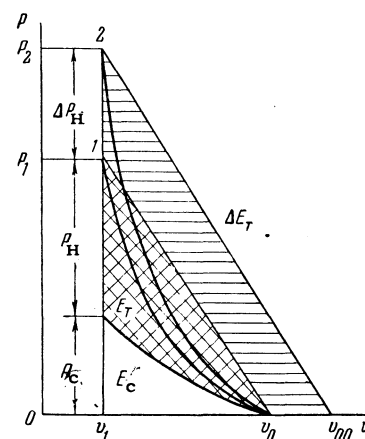


FIG. 1.  $P-v$  diagram of shock compressibility.

this work is transformed into kinetic energy, while the remainder increases the specific internal energy by the amount

$$E(P_1; v_1) = \frac{1}{2} P_1 (v_0 - v_1). \quad (2)$$

Equation (2) describes the Hugoniot adiabat of the shock compressibility of the medium.

The internal energy acquired through compression is divided into an elastic component  $E_c$  represented by the area between the horizontal axis (of volumes) and the curve of  $P_c$ , which is the "cold" compressibility at absolute zero, and the thermal energy  $E_T$  represented by the area of

the crisscrossed curvilinear triangle. Thus a shock compression is always accompanied by heating of the substance and increase of its entropy, which in turn leads to the appearance of a thermal pressure component  $P_T$ . With increasing wave amplitude, the thermal energy and thermal pressure of a shock compression rise progressively.

It is obvious that a single dynamic adiabat does not provide sufficient information for obtaining an equation of state. Ia. B. Zel'dovich has shown that much more complete information regarding the behavior of matter at high pressures can be obtained from two shock adiabats with different initial densities. The shock compression of a porous specimen (of lower density) is associated with large volumetric deformation and a large entropy increase as a result. Thus in the  $P-v$  diagram the "porous" shock adiabat is always above the adiabat of the solid material (see Fig. 1). The relative positions of the two adiabats, which correspond to very different degrees of heating, permit the derivation of a semi-empirical equation of state for the test material. Extrapolation leads to the compressibility curve at absolute zero.

The dynamic procedure for the investigation of equations of state was developed by the present authors about ten years ago. The present article describes the principal methods of measuring the dynamic compressibility at high pressures and the results obtained from a study of iron\* in the range from  $4 \times 10^5$  to  $5 \times 10^6$  atm. One of these methods was independently developed by Mallory,<sup>5</sup> Walsh and Christian,<sup>6</sup> Goranson, Bancroft and others<sup>7,8</sup> in investigations of the compressibility of metals including iron. The range of pressures in these investigations was relatively small and did not exceed a maximum pressure of  $4 \times 10^5$  atm; the results which are pertinent to the subject of the present article will be mentioned in the section on the equation of state of iron.

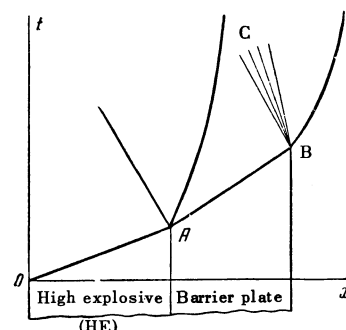
## 1. METHODS OF DETERMINING DYNAMIC COMPRESSIBILITY

The dynamic study of compressibility is based on the experimental determination of wave and mass velocities. Wave velocities are measured relatively simply by contact pins placed in the path of the shock wave. On the other hand, in most cases it is impossible to observe the mass velocity of a substance directly.

We have developed two methods for the complex determination of the kinematic wave parameters,

the method of "splitting off" and the method of "deceleration". The first method studies the propagation of a strong discontinuity which appears in an elastic barrier from which a detonation wave is reflected. Figures 2 with the coordinates path and time represents the motion of the shock wave and unloading wave in the barrier plate. The experi-

FIG. 2.  $x-t$  diagram of the reflection of a detonation wave from an elastic plate. OA - detonation wave; AC - shock wave; BC - centered unloading wave.



mentally measurable quantities are the wave velocity  $D$  and the velocity of displacement  $W$  of the free surface of the plate in the initial portion of its trajectory, which is approximately twice the mass velocity of the material behind the wave front.

The velocity  $W$  is acquired by the matter of the barrier through two different processes; these are, first, the shock transition from the state  $P_0 = 0, v_0$  to the state  $P_1, v_1$  and, secondly, the subsequent isentropic rarefaction in the opposing unloading wave to the state  $P_0 = 0, v'_0 > v_0$ .

In the state  $P_1, v_1$ , the mass velocity is  $U_1 = \sqrt{P_1(v_0 - v_1)}$ . The additional velocity acquired through rarefaction to  $v'_0$  is

$$U'_1 = \int_{v'_0}^{v_1} \sqrt{-dP} dv.$$

For very weak shock waves down to sound waves  $U_1 = U'_1$  and  $W = 2U_1$ . In the general case  $U'_1 \neq U_1$ , which with increasing wave amplitude leads to violation of the law of doubled mass velocity. But for a broad class of possible equations of state of solids, with degrees of shock compression  $\sigma_1 < 1.4$  the departures from the doubling law are of the order 1–2%. Hereinafter for small compressions we shall assume

$$U_1 \approx \frac{1}{2} W. \quad (3)$$

The same result was obtained in Ref. 6, where the question of violations of the doubling law was regarded under the most general assumptions with respect to the isentropic rarefaction. A special experiment showed that for iron the mass velocity is doubled approximately up to very high shock compressions of  $3.5 \times 10^6$  atm. The "splitting-off" method is entirely unsuited to the investigation of

\*This was actually low-carbon steel with 0.2% carbon.

porous materials, where for weak shock waves  $U_1$  is almost zero.

The "deceleration" method is based on very rigorous premises and can be applied to any materials at pressures and densities as high as desired. In the "deceleration" method a smoothly accelerated "shock driver" strikes a "target" at rest inducing two shock waves which are propagated in opposite directions from the collision surface (Fig. 3). The measurable parameters

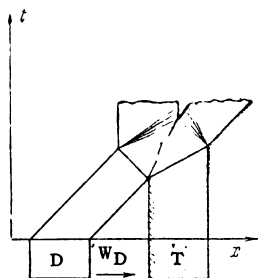


FIG. 3.  $x-t$  diagram of shock deceleration. T is the target; D is the shock driver; 1 is the region of shock compression

are the velocity  $W_H$  of the driver and the velocity  $D_T$  of the shock wave in the "target". In shock compression region 1 on both sides of the driver-target interface equality of velocities and equality of pressures are always established. The first of these equalities follows directly from the continuity of the medium, while the second follows from the law of the equality of action and reaction.

$U_1$  denotes the velocity of progressive motion of the boundary, which coincides with the jump of mass velocity at the front of the shock wave passing through the "target". The velocity jump at the front of the wave propagating through the driver is  $W_D - U_1$ . When the driver and target are made of the same material,  $W_D - U_1 = U_1$  and thus

$$U_1 = \frac{1}{2} W_D. \quad (4)$$

The other parameters of the shock wave in the target are obtained by substituting  $U_1$  and  $D_T$  into the conservation equations (1). Measurements at different velocities of the shock-producing body determine a number of points on the dynamic adiabat of the tested material and thus on the whole determine the dynamic adiabat of the target and driver material.

Equation (4) superficially resembles Eq. (3). But in the splitting-off method the velocity of the barrier is acquired through two essentially different processes, the shock compression and the subsequent isentropic rarefaction, which furnish approximately identical velocities only for relatively weak shock waves. In the deceleration method, the double reduction of velocity through shock deceleration is exact for velocities of any magnitude

and at any pressures and temperatures of shock compression.

When different solids collide, there is no equality of the velocity jumps in the target and driver. This difficulty is easily overcome if the driver is made of a material with a previously determined dynamic adiabat which furnishes a function relationship between shock compression pressure and the velocity jump  $W_D - U_1$ . In the pressure-velocity diagram (Fig. 4), the dynamic adiabat of

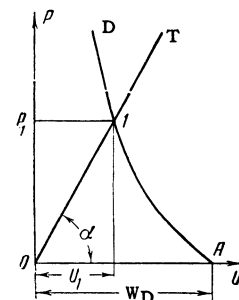


FIG. 4.  $P-U$  diagram of shock deceleration. AD is the adiabat of driver deceleration; OT is the wave line of the target; 1 is the state of shock compression.

deceleration of the driver material is represented by a curve whose distance from the coordinate origin is  $W_D$ . Measurement of the wave velocity  $D_T$  in the target determines the position of the wave line OT of possible shock compression states of the target material, satisfying the equation  $P_T = \rho_{OT} D_T U$  ( $\rho_{OT}$  is the initial density of the target material). In actuality, state 1 is realized for equal pressures and velocities of the driver and target on both sides of the interface. This state lies at the intersection of the driver adiabat and the target wave line. The intersection coordinates determine the pressure and mass velocity, and also through Eq. (1a) the shock compression density of the target material.

## 2. METHOD OF INVESTIGATION AND EXPERIMENTAL TECHNIQUE

Measurements of the wave and mass velocities by the splitting-off method were obtained in a series of 6 to 7 experiments which were designed to induce shock waves of identical amplitude in the barriers. Some of the experimental work was de-

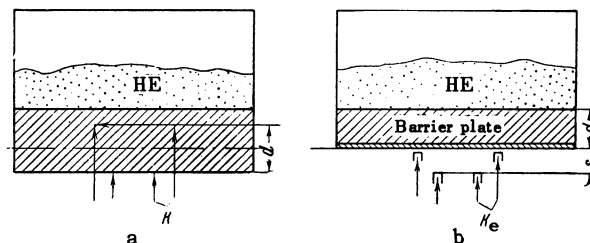


FIG. 5. Scheme of measurements: a - wave velocity; b - splitting-off velocity in the barrier plate. K - electrical contactors;  $K_e$  - electrical contactors with protective caps.

signed to determine the wave velocity according to the scheme of Fig. 5a, and the remainder to determine the velocity of the free boundary according to the scheme of Fig. 5b. The wave measurements are performed by means of two groups of electrical pickups K which are acted upon successively by the shock front. The distance between the "upper" and "lower" pickups provides the measuring base distance  $d$ , which is usually 5 to 8 mm.

With varying velocity of propagation of shock waves, the recording of time intervals furnishes average velocities for the experimental distance; these agree very accurately with the instantaneous shock velocities at the middle of the base distance. Mass velocities behind the shock front must also be measured at the same distance from the explosive. Figure 5 shows that the latter measurements obtained with thinner barriers whose free surfaces are separated from the HE boundary by the same distance as the center of the base distance in the wave measurements.

The velocity of barrier plate motion is not constant (Fig. 2). This is due to the fact that when the detonation wave is reflected at the boundary between the explosive HE and the plate, the pressure and velocity regime which is established decays with time. For a very strong barrier which remains continuous during the initial period of motion the trajectory of the free surface reproduces accurately to within the doubling coefficient and a certain time shift the velocity decay at the detonation interface.

The pattern of motion is complicated by the presence of disruptive stresses in the region occupied by the unloading wave; these stresses are zero on the free surface and have their maximum value at the boundary of the unloaded zone. The magnitude of the stresses increases as the unloading wave moves farther into the barrier. At a certain distance from the surface the tensile stresses reach the limit of dynamic breaking strength; this leads to the formation of a crack and the splitting off of a thin plate. For matter with vanishingly small strength, the split-off plate is very thin. Under such conditions it can be assumed that its velocity coincides with the free surface velocity at the instant when the shock wave reaches it. For the majority of materials, correct values of the initial velocity can be obtained in barriers with a generated surface of separation between the main plate and a split-off plate a few tenths of a millimeter thick (Fig. 5b). Such plates, which separate freely from the main plate, determine our required maximum mass velocity on the shock front as it

reaches the free surface.

In order to obtain undistorted results, the measuring units must be placed close to the explosive axis in a region which is not touched by unloading waves from the lateral surfaces of the explosive charge or the specimen.

Certain limitations are placed on the ratio between the thickness  $d$  of the barrier and the distance  $s$  which is the base for measurement of the surface velocity (Fig. 5b). During a measurement, the unloading wave after reflection from the boundary between the barrier and explosive products must not again reach the free surface. This condition will be fulfilled if

$$s/W \leq 2d/D. \quad (5)$$

In Eq. (5) it is assumed that the velocity of the unloading wave in the barrier is approximately equal to the velocity  $D$  of the transmitted shock wave.

In investigations of relatively strong shock waves, which communicate velocities of a few kilometers per second to the free surface, the electrical pickups K outside the barrier must be covered with special protecting caps that are separated from the contact points by a few tenths of a millimeter. These are required to prevent premature shorting of the electrical contacts by the air shock wave which moves ahead of the barrier plate.

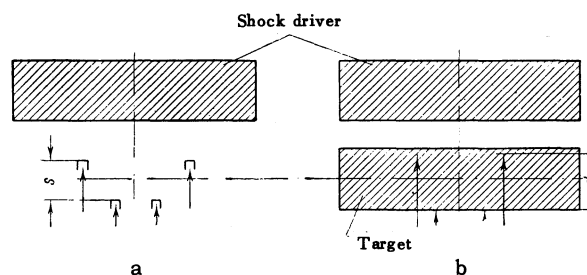


FIG. 6. Arrangement for measurement of wave and mass velocities by the deceleration: a—of the shock driver; b—of the shock wave in the target.

Figure 6 shows the arrangements for determining the velocity of the shock driver and of the wave in the target by the deceleration method. Each of these quantities is determined in an independent series of experiments. With varying, increasing velocity of the driver the wave velocities in the target material and the driver velocities must be measured at an identical point of the trajectory, which is the middle of the measuring base.

Rigorously related values of  $W_D$  and  $D_T$  could be obtained only if the measuring base were made infinitely small, with the target surface at the midpoint  $s$ , and if wave velocities were meas-

ured directly on the surface. This is, of course, impossible. For a finite measuring base distance as shown in Fig. 6b. The motion of the shock driver from the target surface to the center of the base is replaced in wave measurements by the motion of the shock wave in the target. Since the velocity of the driver moving through air and the mass velocity in the shock wave moving through the target do not have identical relative increments, small corrections are made to the measured values of the wave velocities not exceeding one percent of the value of  $D_T$ . As in the splitting-off method, during measurements of  $W_D$  the electrical contactors must be shielded.

In all of the experiments for the determination of wave and mass velocities, time intervals were measured by means of cathode ray oscilloscopes with high sweep velocity; signals from the contactors were fed to the deflecting plates. Figure 7 is a typical oscillogram as recorded with a twin-beam oscilloscope using a method devised by N. N. Lebedev, E. A. Etingof and M. S. Tarasov. The first

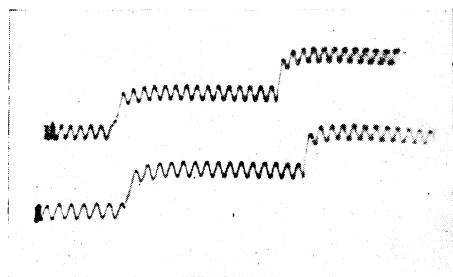


FIG. 7. Oscillogram recording time interval between electrical contacts.

step upward of the traces fixes the time of closing of the upper contacts; the second step upward does the same for the lower contacts. A sine wave with a period of  $10^{-7}$  sec was applied to each beam. Time intervals were recorded with an accuracy of  $\pm 5 \times 10^{-9}$  sec.

We can now estimate the accuracy of determina-

tion of the dynamic compressibility. Differentiating Eqs. (1a) and (1b) with respect to  $D$  and  $U$ , and assuming the relative errors of the wave and mass velocities to be independent of each other, we obtain the following expressions for the root mean square relative errors of  $P$  and  $\sigma$ :

$$\frac{\Delta P}{P} = \pm \left( \sqrt{\left( \frac{\Delta U}{U} \right)^2 + \left( \frac{\Delta D}{D} \right)^2} \right), \quad (6)$$

$$\frac{\Delta \sigma}{\sigma} = \pm (\sigma - 1) \sqrt{\left( \frac{\Delta U}{U} \right)^2 + \left( \frac{\Delta D}{D} \right)^2} \quad (7)$$

Every value of  $D$  and  $U$  was obtained by averaging data from 3 to 4 experiments, in each of which the measurements were repeated a few times. The relative error is  $\pm 0.01$ . When this value of  $\Delta U/U$  and of  $\Delta D/D$  is substituted in (6) and (7) we find that the density spread at  $\rho = 1.5$  and  $2.0\rho_0$  is  $\pm 0.01$  and  $\pm 0.03\rho_0$ , respectively. Pressures were measured with 1.5–2% accuracy.

### 3. DYNAMIC ADIABATE OF IRON

Up to pressure of  $1.5 \times 10^6$  atm, the dynamic adiabat of iron was obtained by both the splitting-off method and the deceleration method. From  $1.5 \times 10^6$  to  $5 \times 10^6$  atm, only the deceleration method was used. Table I contains the parameters of all the experimentally determined points of the shock adiabat of iron. The points are numbered and the methods of measurement are indicated in the first and second column, respectively. The kinematic characteristics of the shock waves are then given: wave and mass velocities in km/sec, pressures in bars, relative shock compressions  $\sigma = v_0/v_1$  and densities in  $\text{g/cm}^3$ . The initial density of the low-carbon steel specimens was  $7.85 \text{ g/cm}^3$ . The highest mass velocity  $U = 5.17 \text{ km/sec}$  corresponds to shock wave velocity  $D = 1200 \text{ km/sec}$ , iron density  $\rho = 13.79 \text{ g/cm}^3$  and pressure  $P = 4.87 \times 10^{12} \text{ bars}$ .

In the entire investigated velocity range from

TABLE I

No. of point	Method of measurement	D, km/sec	U, km/sec	$P \times 10^{12}$ bars	$\sigma = v_0/v_1$	$\rho$ , g/cm <sup>3</sup>
1	Splitting-off	5.30	0.97	0.40	1.224	9.61
2	"	5.38	1.00	0.422	1.228	9.64
3	Deceleration	5.54	1.14	0.50	1.259	9.88
4	Splitting-off	7.27	2.26	1.29	1.451	11.39
5	"	7.54	2.38	1.41	1.461	11.47
6	Deceleration	8.89	3.25	2.27	1.576	12.37
7	"	9.36	3.56	2.62	1.614	12.67
8	"	9.98	3.83	3.00	1.623	12.74
9	"	10.45	4.20	3.44	1.672	13.13
10	"	10.67	4.32	3.62	1.680	13.19
11	"	11.10	4.59	4.00	1.705	13.38
12	"	11.32	4.83	4.29	1.744	13.69
13	"	12.00	5.17	4.87	1.757	13.79

$U = 1.0$  to  $U = 5.17$  km/sec the velocities are related linearly:

$$D = 3.80 + 1.58 U. \quad (8)$$

The functional relations between  $D$  and  $U$ , including the form  $D = C'_0 + \lambda U$ , completely determine dynamic adiabates. For the coordinates pressure and velocity Eq. (8) leads to

$$P = \rho_0 (C'_0 + \lambda U) U.$$

With pressure and the specific volume as coordinates, the linear relation between  $D$  and  $U$  corresponds to the equation of the adiabates:

$$P = \frac{C_0'^2 (v_0 - v)}{(\lambda - 1)^2 v^2 [(\lambda / \lambda - 1) - (v_0 / v)]^2}, \quad (9)$$

which is valid for iron from  $3 \times 10^5$  to  $5 \times 10^6$  atm.

Figure 8 shows the adiabat of iron in the coordinates  $P$  and  $\sigma = v_0/v$ . It must be mentioned that the parameter  $C'_0$  in (9) is an adjusting constant and is not at all related to the actual velocity of propagation of weak acoustic waves.

All of the data refer to the compression of specimens of normal density. Two series of experi-

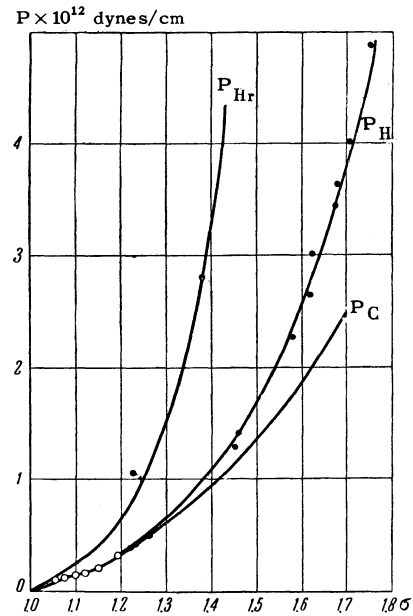


FIG. 8. Shock adiabats and cold compressibility curve of iron.  $P_H$  — shock adiabat of iron at normal density;  $P_{Hr}$  — shock adiabat of iron at reduced density with  $v_{00} = 1.412 v_0$ ;  $P_C$  — isotherm of iron at  $T = 0^\circ$ ; ● — experimental points; ○ — data of Goranson, Bancroft et al.<sup>7,8</sup>

TABLE II

$\rho_0$ , g/cm <sup>3</sup>	$v_0$ , cm <sup>3</sup> /g	$D$ , km/sec	$U$ , km/sec	$v$ , cm <sup>3</sup> /g	$P$ , 10 <sup>12</sup> bars	$E$ , 10 <sup>10</sup> erg/g	$\gamma$	$h$
5.52	0.181	6.69	2.82	0.104	1.05	4.04		
7.85	0.127	—	—	0.104	0.40	0.466	1.95	2.11
5.57	0.181	10.17	4.95	0.0923	2.80*	12.14		
7.85	0.127	—	—	0.0923	1.00*	1.75	1.6	2.25

\*Calculated using Eq. (9).

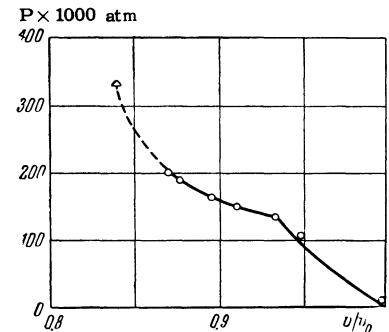


FIG. 9. Compressibility of iron up to 300,000 atm Δ — data from Ref. 7; ○ — data from Ref. 8.

ments were performed with specimens of reduced density. The results of the latter, which were obtained by the deceleration method, are given in Table II, which also contains for comparison the greatly reduced values of  $P$  and  $E$  that were obtained through a shock compression to the same densities of solid iron. The dimensionless parameters  $\gamma$  and  $h$  are also given; these will be discussed below.

#### 4. COMPRESSION OF IRON AT ABSOLUTE ZERO

There is undoubted interest in the transition from shock compressions where an important part is played by the thermal components of the pressures to the relation  $P_C(v)$  at absolute zero.

Goranson and Bancroft and their collaborators<sup>7,8</sup> have studied the compressibility of iron below 300,000 atm. Of special interest are the results of Bancroft et al.,<sup>8</sup> who at 132,000 atm discovered a phase transition accompanied by a kink in the compressibility curve (Fig. 9). Since the thermal components of the pressures are still small at this pressure, the data obtained in Refs. 7 and 8 can be used directly for the purely cold compression relation  $P_C(v)$ . By treating the curve of Fig. 9 as  $P_C$ , we obtain the cold compression energy  $E_C$  through a volume integration of this curve. The values of  $E_C$  and  $P_C$  for  $P < 0.3 \times 10^6$  atm are given at the beginning of Table III.

We now turn to the deduction of the equation of state of iron, which we need for the cold compres-

TABLE III

$v_0/v$	$E_c \cdot 10^{10}$ , erg/g	$P_c \cdot 10^{13}$ , bars	$P_H \cdot 10^{13}$ , bars
1.07	0.0525	0.132*	
1.15	0.181	0.200*	
1.19	0.30	0.332**	
1.25	0.585	0.463	0.484
1.30	0.86	0.600	0.645
1.35	1.18	0.761	0.840
1.40	1.57	0.942	1.07
1.45	1.97	1.154	1.36
1.50	2.42	1.358	1.67
1.55	2.94	1.613	2.08
1.60	3.51	1.880	2.55
1.65	4.12	2.174	3.13
1.70	4.79	2.484	3.82
1.75	5.54	2.822	4.66

\*From Ref. 8.

\*\*From Ref. 7.

sibility at high shock compression densities, where the dynamic adiabat differs considerably from the isotherm at absolute zero. Here and hereinafter, we shall not distinguish between isotherms at room temperature and at absolute zero.

We shall write the equation of state and an expression for the internal energy in the form

$$P = -\partial E_c / \partial v + BT/v; \quad (10)$$

$$E = E_c + C_v T. \quad (11)$$

Here  $-\partial E_c / \partial v = P_c$  is the compression pressure at  $T = 0^\circ K$ ,  $B$  is the thermal pressure coefficient,  $C_v$  is the specific heat at constant volume. In general,  $B$  and  $C_v$  can depend on temperature and density.

When temperature is eliminated we obtain the well-known caloric equation of state<sup>9-10</sup>

$$P + \frac{\partial E_c}{\partial v} = \gamma \frac{E - E_c}{v}. \quad (12)$$

The left member of (12) is the thermal component of the pressure and the ratio  $(E - E_c)/v$  in the right member is the volumetric density of thermal energy.

The Grüneisen coefficient  $\gamma = B/C_v$  gives the ratio of the thermal pressure to the thermal energy density. We shall consider this quantity to be a constant which like the unknown function  $E_c(v)$  must be obtained from experiment. For this purpose, substituting in (12) the expression for  $E$  given by the Hugoniot equation (2), we obtain the differential equation

$$v \frac{\partial E_c}{\partial v} + \gamma E_c = -\gamma \frac{P_H(v)v}{2} \left( 1 + \frac{2}{\gamma} - \frac{v_0}{v} \right). \quad (13)$$

When  $v_1 = v_0$ ,  $E_c = \partial E_c / \partial v = 0$ . In (13)  $P_H(v)$  is the experimental equation of the shock adiabat. The solution of (13) is given by

$$E_c = \frac{1}{(h-1)v^{2/(h-1)}} \int_{v_0}^v P_H(x) \left( \frac{v_0}{x} - h \right) x^{2/(h-1)} dx, \quad (14)$$

$$P_c = -\frac{\partial E_c}{\partial v} = \frac{2}{(h-1)^2 v^{(h+1)/(h-1)}} \quad (14a)$$

$$\times \int_{v_0}^v P_H(x) \left( \frac{v_0}{x} - h \right) x^{2/(h-1)} dx - \frac{1}{h-1} P_H(v) \left( \frac{v_0}{v} - h \right).$$

In (14)  $h = (2/\gamma) + 1$  is the so-called maximum density of shock compression.

At pressures from  $3 \times 10^5$  to  $5 \times 10^6$  atm,  $P_H(v)$  for iron is given by (9). We shall be committing only a very small error if, when calculating  $E_c$  in the region  $P > 3 \times 10^5$  kg/cm<sup>2</sup>, we consider (9) to apply also to the initial portion of the dynamic adiabat.

In order to determine  $\gamma$  and thus  $h$ , we shall compare two states 1 and 2 representing the shock compression of solid and of porous iron, respectively, to the same specific volume  $v_1$  (Fig. 1). Since both states have the same energy  $E_c$ , which depends only on the volume, the pressure difference  $\Delta P = P_2 - P_1 = \Delta P_T$  is accounted for by the thermal energy difference  $\Delta E = E_2 - E_1 = \Delta E_T$ . From (2)

$$\Delta E_T = \frac{1}{2} [P_2(v_{00} - v_1) - P_1(v_0 - v_1)]. \quad (15)$$

Here  $v_{00}$  is the initial volume of the porous iron and  $P_2$  is the shock compression pressure of the porous iron. The constants  $\gamma$  and  $h$  are obtained on the basis of (15) from the equations

$$\frac{1}{\gamma} = \frac{\Delta E_T}{v_1 \Delta P_T} = \frac{1}{2} \left[ \frac{v_{00} P_2 - v_0 P_1}{(P_2 - P_1) v_1} - 1 \right]; \quad (16)$$

$$h = \frac{(v_{00}/v_0) P_2 - P_1}{P_2 - P_1} \left( \frac{v_0}{v_1} \right). \quad (16a)$$

The available experimental data on the dynamic compressibility of porous iron (in Table II) permit us to obtain  $\gamma$  and  $h$  for two degrees of shock compression. The values of these parameters are given in the last two columns of Table II. For the transition from the dynamic adiabat to the isotherm  $T = 0$ ,  $h$  is more important at high compressions, that is, in the region where the thermal components of the pressures are relatively large. In subsequent calculations, we shall assume  $h = 2.25$ .

The values of the cold compression energy  $E_c$  and of the pressure  $P_c = -\partial E_c / \partial v$  calculated from (14) are given in Table III for pressures from 0.3 to 5 million atmospheres. Also given are the pressures  $P_H(v_0/v)$  of the shock adiabat for the compression of iron of normal density, which were calculated from the interpolation formula (9).

Knowing the function  $E_c$  and its derivative, we

can now write an expression for the adiabat of shock compression from a state with the initial volume  $v_{00} \geq v_0$ . Solving (13) with respect to  $P_H$ , we obtain

$$P_H(v_{00}; v) = - \frac{(h-1) \partial E_c / \partial v + 2E_x / v}{h - v_{00}/v} = \frac{(h-1) P_c - 2E_c/v}{h - v_{00}/v}. \quad (17)$$

The curve  $P_c$  of cold compressibility, the experimental adiabat of solid iron (9) and the adiabat of porous iron with initial volume  $v_{00} = 1.412 v_0$  are compared in  $P-v$  diagrams (Fig. 8). Thermal pressure plays a strikingly large part, especially in the shock compression of porous iron.

We note in conclusion that the equation of state (12) and the expressions that have been found for  $\gamma$  and  $E_c$  are valid in the region bounded by the curve for cold compressibility  $P_c$  and the shock adiabat of porous iron.

## 5. EXTRAPOLATION OF THE COMPRESSIBILITY CURVE OF IRON

The compressibility of matter at absolute zero can be studied by quantum statistical methods. However, the Thomas-Fermi and Thomas-Fermi-Dirac statistical models of the atom hold true only at very high pressures of hundreds of millions of atmospheres, when the electronic shells of the atoms are pressed together and lose their individual structure.<sup>11</sup>

At relatively low compression up to 2 or  $3\rho_0$  statistical methods yield highly exaggerated values of the pressures. Figure 10 is a logarithmic plot for iron of density-pressure curves which were computed by the Thomas-Fermi method<sup>11</sup> and by the Thomas-Fermi-Dirac method,<sup>11</sup> with an exchange correction. According to Kompaneets and Pavlovskii,<sup>13</sup> the Thomas-Fermi-Dirac results are correct when the exchange correction is small, which undoubtedly occurs for compression close to  $\rho = 8 - 10\rho_0$ . The lower branch of the compressibility curve up to  $\rho = 1.7\rho_0$  has been obtained experimentally by the present authors.

From a knowledge of the upper and lower portions of the function  $P_c(\rho)$  we are able to interpolate it satisfactorily for the intermediate region from  $\rho = 1.7\rho_0$  to  $\rho = 8\rho_0$  (see the dashed line in Fig. 10). The same graph shows Jensen's interpolation,<sup>14</sup> which lies considerably above both the curve for  $P_c$  and the dynamic adiabat. The error in Jensen's curve resulted from the lack of experimental information on the compressibility of iron at pressures of several million atmospheres.

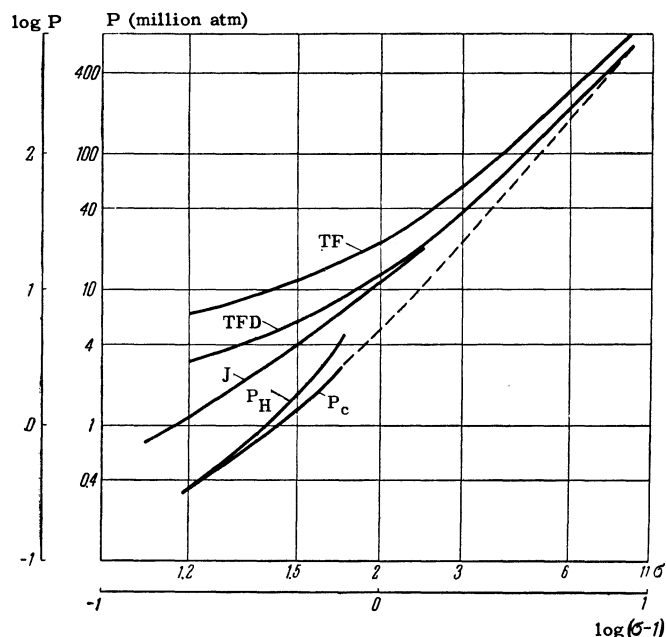


FIG. 10. Extrapolation of the compressibility curve at  $T = 0^\circ\text{K}$ . TF was computed with the Thomas-Fermi model; TFD was computed with the Thomas-Fermi-Dirac model;  $P_c$  is an experimental portion of the isotherm  $T = 0$ ; J is the isotherm  $T = 0$  according to Jensen;  $P_H$  is the experimental dynamic adiabat. The dashed line is the extrapolated portion of the isotherm  $T = 0$ .

## CONCLUSION

Dynamic methods of investigating compressibility greatly broaden the experimental possibilities in high pressure physics. Our deceleration method is especially promising since it enables us to perform measurements up to a few million atmospheres of pressure. We were thus able to determine the dynamic adiabat of iron with different initial densities from  $4 \times 10^5$  to  $5 \times 10^6$  atm.

The dynamic adiabat of porous iron with its reduced initial density lies considerably higher than the adiabat of the solid material in the pressure-density diagram. This is evidence of the large part played by the thermal components of the pressure in shock compression.

On the basis of our experimental findings, we have derived an empirical equation of state for iron and have obtained the cold compressibility curve up to densities  $\rho = 1.7\rho_0$ . The isotherm at  $T = 0^\circ$  has been extrapolated to pressures at which quantum statistical methods of computation are applicable.

The present work was undertaken at the suggestion of Ia. B. Zel'dovich. In methodological and instrumental matters the authors were constantly assisted by V. A. Tsukerman and his co-workers E. A. Etingof, N. N. Lebedev and M. S. Tarasov.



The successful conduct of the investigation was greatly assisted by advice and active participation in discussions on the part of E. I. Zababakhin, S. B. Kormer, E. A. Negin and G. I. Gandel'man. In the initial stages some very valuable experimental information was obtained by D. M. Tarasov and A. A. Bakanova. The numerous complicated experiments were performed with the aid of the technicians A. A. Zhiriakov, S. P. Pokrovskii and A. N. Kolesnikova. The authors are extremely grateful to all of these colleagues.

<sup>1</sup>P. W. Bridgman, The Physics of High Pressure (London, 1931) ONTI, 1936.

<sup>2</sup>P. W. Bridgman, Recent Work in the Field of High Pressures, *Revs. Modern Phys.* **18**, 1 (1946), *Russ. Transl. IIL*, 1948.

<sup>3</sup>P. W. Bridgman, *Proc. Am. Acad. Arts. Sci.* **76**, 3, 55 (1948).

<sup>4</sup>L. D. Landau and E. M. Lifshitz, *Механика сплошных сред (The Mechanics of Continuous Media)*, GITTL, 1953.

<sup>5</sup>H. D. Mallory, *J. Appl. Phys.* **26**, 555 (1955).

<sup>6</sup>M. Walsh and R. H. Christian, *Phys. Rev.* **97**, 1544 (1955).

<sup>7</sup>W. Goranson, D. Bancroft et al., *J. Appl. Phys.* **26**, 1472 (1955).

<sup>8</sup>Bancroft, Peterson and Minshall, *J. Appl. Phys.* **27**, 291 (1956).

<sup>9</sup>E. Grüneisen, *Handbuch der Physik*, 1926, Vol. 10, pp. 1-59.

<sup>10</sup>Ia. I. Frenkel', *Статистическая физика (Statistical Physics)*, Acad. Sci. USSR Press, 1948.

<sup>11</sup>P. Gombas, *Die statistische Theorie des Atoms und ihre Anwendungen* (Wien, 1949).

<sup>12</sup>N. Metropolis and J. R. Reitz, *J. Chem. Phys.* **19**, 555 (1951).

<sup>13</sup>A. S. Kompneets and E. S. Pavlovskii, *J. Exptl. Theoret. Phys. (U.S.S.R.)* **31**, 427 (1956); *Soviet Phys. JETP* **4**, 328 (1957).

<sup>14</sup>H. Jensen, *Z. Physik* **111**, 373 (1938).

# DYNAMIC COMPRESSIBILITY OF METALS UNDER PRESSURES FROM 400,000 TO 4,000,000 ATMOSPHERES

L. V. AL'TSHULER, K. K. KRUPNIKOV and M. I. BRAZHNİK

Submitted to JETP editor December 28, 1957

*J. Exptl. Theoret. Phys. (U.S.S.R.)* **34**, 886-893 (April, 1958)

A method for the determination of pressures and densities of shock compressions is proposed which is based on the measurement of the velocities of propagation of strong shock waves. The dynamic compressibility of copper, zinc, silver, cadmium, tin, gold, lead and bismuth were measured by this method in the pressure range from 400,000 to 4,000,000 atm. The highest degrees of compression (by factors 2.26 and 2.28) were observed in lead and bismuth, which possess the largest atomic volumes. The highest absolute density (32.7 g/cm<sup>3</sup>) was recorded for gold.

## INTRODUCTION

DYNAMIC methods of investigation in high pressure physics are based on the compression of matter by means of strong shock waves. Experimentally measurable parameters of shock waves are  $D$ , the velocity of propagation of a wave front in an undisturbed medium, and  $U$ , the velocity of matter behind the wave front. Having determined

these parameters, from mass and momentum conservation we obtain the density

$$\rho = \rho_0 D / (D - U) \quad (1)$$

and the pressure of a shock compression

$$P = \rho_0 U D. \quad (2)$$

For the complex determination of shock wave parameters we<sup>1</sup> have developed two methods of in-